Finger front propagation in smectic-*A* Fréedericksz transition

Marcel G. Clerc [*] and Gregorio Gonzalez-Cortes [†]
Departamento de Física and Millennium Institute for Research in Optics, Facultad de Ciencias Físicas y Matemáticas, Universidad de Chile, Casilla 487–3, Santiago, Chile

Mauricio J. Morel [‡]
Departamento de Química y Biología, Facultad de Ciencias Naturales, Universidad de Atacama, Avenida Copayapu 485, Copiapó, Chile

Paulina I. Hidalgo [§] and Jorge Vergara [‖]
Departamento de Química Orgánica, Facultad de Ciencias Químicas, Universidad de Concepción, Concepción, Chile

(Received 11 March 2021; revised 2 April 2022; accepted 20 April 2022; published 17 May 2022)

Systems with multistability are characterized by exhibiting complex nonlinear waves between equilibria. Experimentally, near the smectic-*A* to chiral nematic transition in a liquid crystal mixture cell with planar anchoring, we observe finger fronts emerge in the smectic-*A* phase when applying an electric field, a reorientation transition. Finger fronts propagate in the direction orthogonal to the anchoring. Colorimetry characterization allows us to describe the molecular reorientation transition and front dynamics. We reveal that the reorientation transition is of the first-order type and determine their critical points. The front speed is determined as a function of the applied voltage. Theoretically, based on a prototype model of liquid crystal transitions, we qualitatively describe the experimental observations. We have analytically determined the bifurcation diagram and the propagation speeds of finger fronts, finding a fair agreement with the experimental observations.

DOI: 10.1103/PhysRevE.105.054701

I. INTRODUCTION

The coexistence of different equilibria, *multistability*, characterizes macroscopic systems with permanent injection and dissipation of energy [1–4]. Namely, depending on the initial conditions, one observes the different equilibria. The set of initial conditions that end in a given equilibrium characterize its basin of attraction. In general, the curves that separate the different basins of attraction, usually called separatrix, have a complex geometry of a fractal nature [5]. Likewise, in the evolution to a given equilibrium, an arbitrary initial condition, the emergence of domains is observed, that is, a state characterized by the observation of distinct equilibria in different spatial regions. The interface between these domains is usually dominated as a domain wall by its analogy to magnetic systems. The relative stability between equilibria induces these domain walls to propagate so that the most stable state invades the least stable one. These types of nonlinear waves are called fronts [2,3,6,7]. These fronts have been observed in several contexts ranging from biology to chemistry to physics [2–4,6–8]. The front's propagation speed depends on the relative stability and features of the equilibria that it connects [8]. The propagation of fronts in different spatial dimensions has been studied. For one-dimensional systems, the fronts correspond to nonlinear waves that connect two equilibria, which are interpreted as heteroclinic curves of the associated comobile or stationary associated dynamical system [9]. The analytical characterization of the front speed is a complex nonlinear problem [8]. It is generally only accessible close to the point where the two equilibria are energetically equivalent, the so-called *Maxwell point* [3]. At this critical point, fronts are characterized by being motionless. Hence, by modifying a parameter, one can reverse the propagation direction of the front.

The previous scenario changes radically in two spatial dimensions where the speed of propagation is now also controlled by the curvature effects of the interface between the two equilibria. The above phenomenon is known as the Gibbs-Thomson effect (see Ref. [3] and references therein). Even the effects of curvature can destabilize interfaces by generating rich interface morphology [10]. As a result of tip-splitting and side-branching, surprising interfaces such as those observed in snowflakes are generated. Besides, the curvature effects can generate the emergence of the spread of fingers in isotropic systems [11]. These propagative fingers correspond to fronts that preferentially spread in one direction as a consequence of interface curvature and anisotropy.

A natural system that exhibits multistability as phases or reoriented states when subjected to electric, magnetic, and electromagnetic fields and temperature changes are liquid crystals [12,13]. The transition from an oriented to a reoriented state induced by an electric or magnetic field is known as the Fréedericksz transition [14]. Nematic liquid crystals exhibit a supercritical Fréedericksz transition [12,13]. Molecular reorientation transitions are not expected to be

[*] marcel@dfi.uchile.cl
[†] gregorio.gonzalez@ug.uchile.cl
[‡] mauricio.morel@uda.cl
[§] pauhidal@udec.cl
[‖] jovergar@udec.cl

seen in smectic-*A* liquid crystals [15,16] due to the orientational and positional order. Notwithstanding, the reorientation transition has been reported near a smectic-*A* to smectic-*C* transition [17].

The paper aims to study the propagation of finger fronts in a smectic-*A* liquid crystal, which corresponds to a reorientation instability induced by an electric field. Based on a cell of a liquid crystal mixture with planar anchoring near the smectic-*A* to chiral nematic transition, when applying a voltage through the cell, we observed the emergence of thin finger fronts that propagate in the direction orthogonal to the anchoring conditions. We use colorimetry characterization to describe the molecular reorientation transition and front dynamics in a liquid crystal cell [18]. This allows us to reveal that the reorientation transition is of the first-order type. The critical points that characterize the transition are established. The fronts connect two stable orientational states. Besides, the colorimetry characterization enables us to characterize the propagation speed as a function of the voltage in different orientations. Theoretically, we have considered a prototype model of transitions in liquid crystals, which qualitatively describes the experimental observations. We have analytically described the bifurcation diagram and the propagation speeds of the finger fronts.

II. LIQUID CRYSTAL MIXTURE

The most common liquid crystals are composed of rodlike organic molecules [12,13], which, as a result of intermolecular interaction, for specific temperature ranges are arranged to have a similar molecular orientation. These molecules can only exhibit an orientational order (nematic liquid crystal) or also have a positional one (smectic liquid crystal). This self-organization generates a strong anisotropy of all its physical properties, similar to those observed in anisotropic crystals, especially the optical ones. Also, due to the lack of rigid positional order, these materials can flow. Liquid crystals are interesting for their intriguing fundamental properties and applications in our daily lives, like cosmetics and interfaces between us and electronic devices. In particular, liquid crystal displays are the most common displays in the last decades [19]. All these technological advances have been possible thanks to the use of molecule mixtures in a crystalline liquid state. Liquid crystal mixtures can permit mesomorphic range control, electric or magnetic features, and optical properties.

A. Phase diagram of E7 and EOS-12 mixture

To carry out our study of finger front propagation in the smectic-*A* Fréedericksz transition, we have considered a liquid crystal mixture based on a commercial liquid crystal E7 (Merck) and a chiral molecule EOS-12 and that synthesized in Ref. [20]. Figure 1 shows a chemical structure of EOS-12, where it is possible to appreciate the chiral centers responsible for the cholesteric phase. EOS-12 is miscible for all concentrations in the matrix of E7. The phase diagram is presented in the range between 10 and 30 wt %. Figure 1 displays the temperature-concentration phase diagram. For sufficiently high temperatures, over 60 °C, we do not observe that the mixture exhibits a mesoscopic order; therefore, the mixture

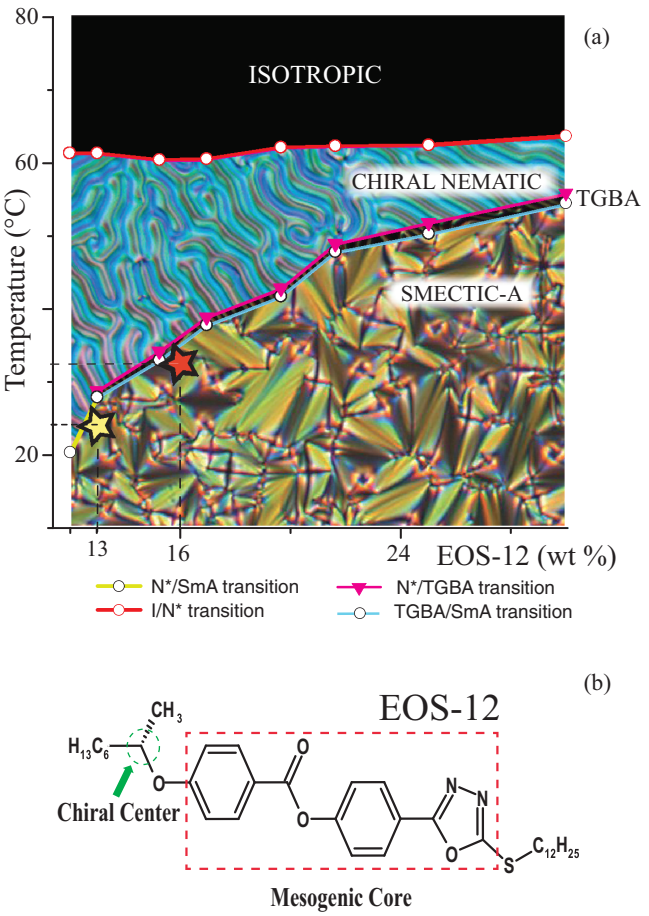

FIG. 1. Liquid crystal mixture. (a) Phase diagram of a liquid crystal mixture based on a commercial liquid crystal E7 and a chiral molecule EOS-12. The horizontal and vertical axes account for EOS-12 concentration and temperature, respectively. The respective snapshots of the zones account for the typical images observed using polarized optical microscopy. The different curves account for the transitions between the different phases. The yellow star shows the point (13 wt %, 24 °C) at which the finger front propagation is studied. A similar analysis is also performed for concentration 16 wt % and temperature 32 °C, represented by the red star. (b) Chemical structure of EOS-12.

behaves as an isotropic liquid (*I*) [12,13]. Using polarized optical microscopy [21], the mixture in this parameter region is entirely dark. As the temperature decreases, we observe a subcritical transition to a chiral nematic phase (N^*); that is, the molecules exhibit an orientational ordering that, in turn, as one moves through the liquid crystal sample the orientation rotates (chirality) [13]. The violet curve with circles shows the chiral nematic isotropic transition, I/N^* transition, in Fig. 1. Besides, this type of phase is characterized by exhibiting labyrinthine textures, as illustrated in Fig. 1. The observed labyrinths are glassy according to the classification used in Ref. [22]. From the chiral nematic state N^* and low concentrations of EOS-12 when lowering the temperature, we observe a supercritical transition to a smectic-*A* state (Sm*A*). Figure 1 depicts the typical texture of the Sm*A* phase [23]. The N^*-Sm*A* transition is accounted for by the yellow curve in Fig. 1. For higher concentrations of the chiral molecule,

we observe that the nematic chiral to smectic-*A* transition is of the subcritical type, and also a phase is observed that corresponds to oriented terraces that rotate (TGBA), which correspond to a frustrated mesophase [24]. This phase is only observed by lowering the temperature and exists in a small temperature range in the order of 1 °C. The region where the TGBA is observed is enclosed between the violet and the cyan curve (cf. Fig. 1). The values of the elastic constants, dielectric anisotropy, and rotational viscosity of the E7 and EOS-12 mixtures have not yet been characterized. The response of the liquid crystal mixtures to an electric field is characterized by having a positive dielectric anisotropy.

B. Fréederickz transition

To understand the behavior of liquid crystals under external electric and magnetic fields, they are usually sandwiched between two rectangular sheets of transparent glass. The glass surfaces are suitably treated with polymers to induce a precise orientation of molecules, *anchoring*. By elastic coupling, all molecules are oriented to satisfy the anchoring conditions. An electric field can be applied orthogonally to the cell by using transparent electrodes adhered to the glass layers. For large enough applied voltage, in the case of positive (negative) dielectric anisotropic susceptibility, the molecules try to reorient parallel (orthogonal) to the applied electric field. The molecules are not reoriented for small voltages due to the interaction induced by the surface anchored molecules, *elastic coupling*. The critical value from which the molecular reorientation is generated corresponds to the Fréederickz voltage (V_{FT}) [14]. Nematic liquid crystals are characterized by exhibiting a supercritical Fréederickz transition [12,13]. However, when the Fréederickz transition is driven by optical feedback [25], through the simultaneous application of electric and magnetic fields [26–28] or through the action of an optical field [29,30], it is of the subcritical type. The above scenario completely changes in the case of smectic-*A* liquid crystal cells. When one applies an electric field, one does not expect to see molecular reorientation [15,16]. It is not expected that an elastic distortion should occur when an electric field is applied because the elastic deformation would destroy the terrace structures of the smectic-*A* phase [15,16]. However, near a smectic-*A* to smectic-*C* transition, the possibility of a reorientation transition induced by an electric field has been observed [17]. This Fréedericksz transition is due to the interlayer spacing, and the packing structure of the smectic layering near the transition begins to lose its rigidity. Depending on the thickness of the liquid crystal cell, the transition from nematic to smectic-*A* can be of the first or second-order [31]. The smectic liquid crystals doped by ferroelectric nanoparticles also exhibit reorientation instabilities [32].

In the next subsection, we study the reorientation transition of the liquid crystal mixture near the smectic–nematic-chiral transition.

C. Experimental setup

As we have mentioned, we have used a mixture of two components, EOS-12 and E7. The first component was synthesized and characterized following the procedure according to Ref. [20], the IUPAC name of EOS-12 corresponds to (*S*)-(4-(5-dodecylthio-1,3,4-oxadiazole-2-yl) phenyl 4′-(1″-methylheptyl-oxy)benzoate). On the other hand, E7 is a commercial mixture acquired from INSTEC Inc. and was used without further purification. Binary mixtures were prepared by weighing each component (EOS-12 and E7) and dissolving separately into methylene chloride. The solution was combined and homogenized by sonicating for 5 min. The solvent was removed by slow evaporation at room temperature. The planar-nematic cell was prepared by introducing the liquid crystal mixture by capillarity in the cell. The cell has a thickness of $d = 3.2 \pm 0.3$ μm and an electrode area of 25 mm^2 of ITO with a thickness of 0.023 μm, a resistance of 100 Ω, and a polyimide thickness of 0.06 μm. Likewise, cells have a homogeneous alignment layer with a 1° to 3° pretilt angle from the plane of the substrate.

The phase diagram and finger fronts were characterized by polarized optical microscopy (POM). The phase diagram was obtained by putting a specific concentration into two glasses without surface treatment. The transition temperatures and textures of mesophases were determined by POM using an Olympus BX51 optical microscope equipped with an Olympus U-TV0.5XC-3 polarizer and a LinkamT95-PE hot stage. The whole study of finger fronts was conducted in a liquid crystal mixture with a concentration of 13 wt % of EOS-12 in E7 at 24 °C. The liquid crystal was introduced into planar cells. The temperature was controlled by a thermal control stage with four electrical connectors (Linkam Mod. TST350E). The voltage was generated by a wave-form modulator coupled to an oscilloscope with a sinusoidal wave form (Agilent 33500B series) and coupled to an amplifier (Tabor Electronics 9400). The colorimetry analysis was developed from a Leica microscope (DM2700P) with a Complementary Metal Oxide Semiconductor camera (CMOS, Thorlabs-DCC1645). Figure 2(a) shows a schematic representation of the experimental setup, where the temperature conditions are controlled by a thermal stage and connected to the wave-form generation system. The schematic representation of the liquid crystal cell and the front propagation are shown in Fig. 2(b), where it is possible to observe the molecular reorientation associated with the finger fronts. In this representation, the rubbing direction that is orthogonal to the preferential direction of the front is marked.

The finger front propagation was obtained from a transparent cell under an applied voltage with a sinusoidal wave form and a frequency of 1 kHz. The voltage was increased slowly, and a CMOS camera recollected images and video. The microscope has a configuration of parallel polarizers (also can be observed by cross-polarizer), and the cell is putting with the rubbing direction to 45° to the polarizer [see symbol *R* in Fig. 2(b)]. Figure 3 shows the evolution of the finger fronts on time. Fingers are mostly originated from imperfections (glass beads or border of the electrodes) such as is shown in Fig. 3(b). Transversal ($V_{\perp}$) and longitudinal ($V_{\parallel}$) speeds also can be determined by taking the displacement (in pixels) at different times. The spatiotemporal diagram is incorporated as much as transversal and longitudinal displacement of the fronts. Note that from spatiotemporal diagrams one can observe the difference between propagation magnitudes

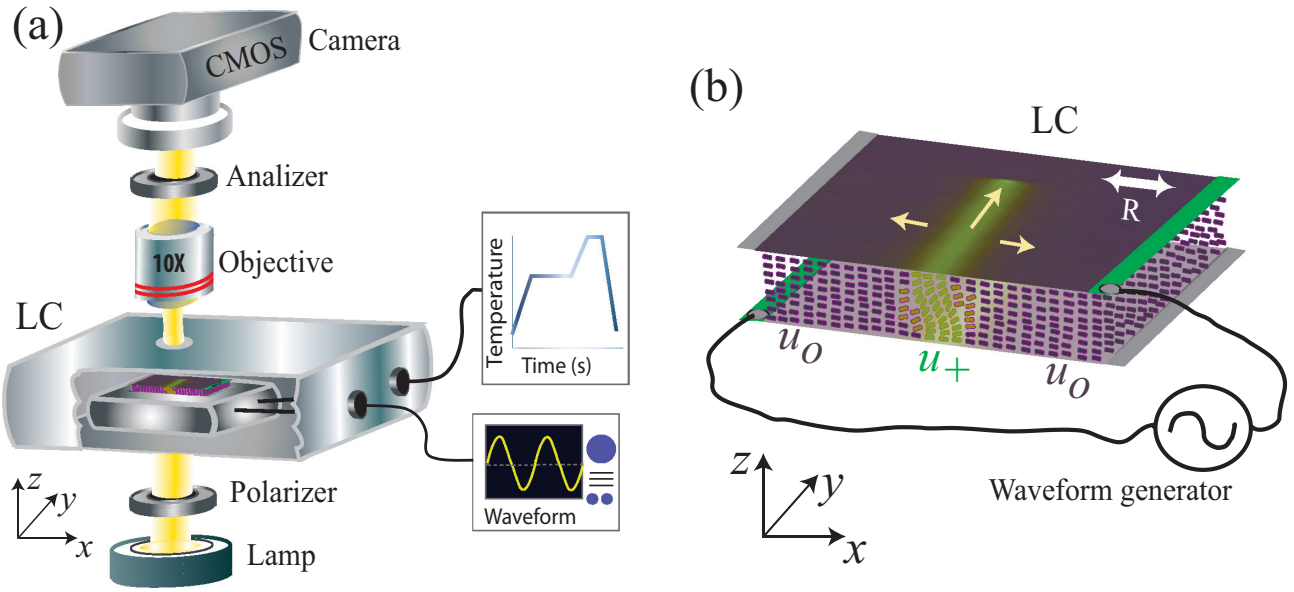

FIG. 2. Schematic representation of the experimental setup. (a) Description of the experimental setup indicating the microscope and the thermal stage with electrical connections joined to the thermal controller and a wave-form generator. Inside the thermal stage, we show the liquid crystal cell and the CMOS camera. (b) Three-dimensional schematic representation of the liquid crystal cell under the influence of the electric field where it is possible to observe the molecular reorientation. The rods and the colors account for the molecular orientation and their angle with respect to the glass layers. The arrows stand for the direction of propagation of the front. u_0 and u_+ account for planar and reoriented states. The anchoring direction of the molecules is described by R.

in each direction. Figure 4 illustrates a sequence of magnified snapshots showing how the front propagates in both directions, parallel and orthogonal to the anchoring.

The bifurcation diagram is obtained using the hue from the conversion RGB to HSL system, according to the procedure used in Ref. [18]. The images selected to be analyzed are taken from a zone where the fronts are semistationary but constant in hue with respect to time. This is corroborated from a hue versus frames and determined the linearity (minimum square method) and the standard deviation for each value. Figure 5 shows the curve obtained from a video taken at 3.9 Vrms. We took the last 500 images (frames) with a standard deviation of 0.096 31° in hue for this graph. For a better interpretation of the results, 360° is added to the hue value associated with the finger front, and after that is rest the minimum value of the hue. We call this physical magnitude Hue°. The speeds are determined by graphing of displacement of the fronts versus time. This analysis was developed using the gray scale because of better contrast.

D. Experimental results

The bifurcation diagram in the smectic-*A* Fréedericksz transition is obtained by changing the voltage applied to the liquid crystal cells and monitoring the evolution of hue employing the CMOS camera. Figure 6 shows the bifurcation diagram and transversal and longitudinal speed as a function of the applied voltage. When the voltage is below the V_{FT}, the molecules are not reoriented; the hue observed is around red-purple. The finger fronts are observed when the voltage reaches a critical value of 3.825 Vrms (V_{FT}) to a temperature of 24 °C. At this moment, the hue is around green-yellow. The preferential propagation direction of the fronts appears as a consequence of molecular reorientation. The front propagation has an opposed sense to the rubbing of the cell [cf. Figs. 1(b) and 3(b)]. Molecular reorientation of the smectic-*A* means a transition of the first order, where the change of hue is abrupt in the scale of degrees (80°). Above V_{FT}, the hue is slightly increased (40°) when the voltage increases from 3.825 to 4.200 Vrms. When the voltage is lowered to voltage V_{SN} (3.298 Vrms), the hue is slightly modified. Any further decrease will trigger an abrupt change in the hue. The hysteresis loop and a bistability zone are identified (cf. Fig. 6).

An anisotropic behavior characterizes the observed fronts. Namely, they present a preferential direction of displacement (cf. Fig. 4). Figure 6 shows the difference of transversal and longitudinal speed as a function of the voltage. When the voltage increases, both front speeds increase; however, the transversal speed increases more slowly. This dynamic behavior is responsible for the emergence of propagating fingers. When the voltage is diminished below V_{FT} and reaches the value of 3.6 Vrms, the longitudinal speed has a value close to zero. The results presented for finger fronts are obtained at a fixed temperature of 24 °C and a 13 wt % of EOS12. However, for different temperatures and concentrations close to the smectic-*A* to cholesteric transition (yellow, violet, and cyan curves in Fig. 1), the emergence and similar dynamical behaviors of finger fronts is observed. In particular, a careful

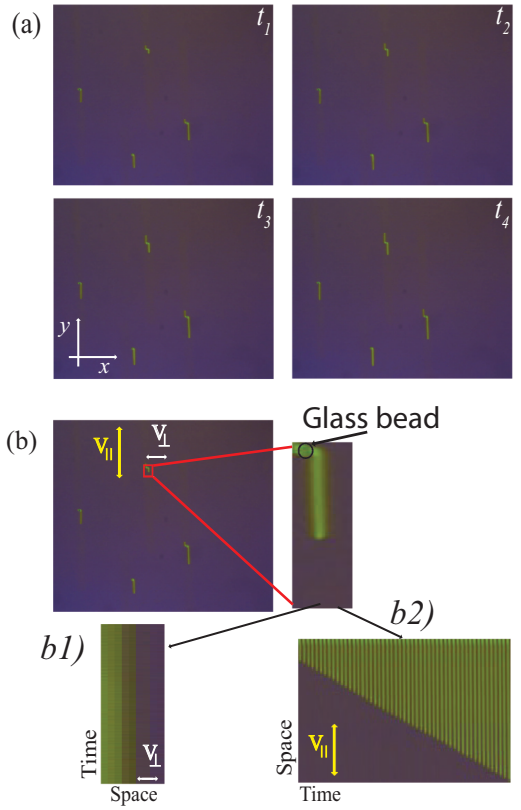

FIG. 3. Experimental front propagation. (a) A sequence of snapshots for different instants ($t_1 < t_2 < t_3 < t_4$). The red-purple and green-yellow color account for the smectic and the reoriented molecular state. (b) Emerging front of a glass bead. $V_\perp$ and $V_\parallel$ account for the speed of propagation of the fronts parallel and orthogonal to the anchoring direction. Taking an extract from the snapshot, one can observe the emergence and propagation of the front (b1). (b2) From this extract, one can generate a regular temporal sequence of the evolution of the fingers, which illustrates the speed of propagation of these fingers.

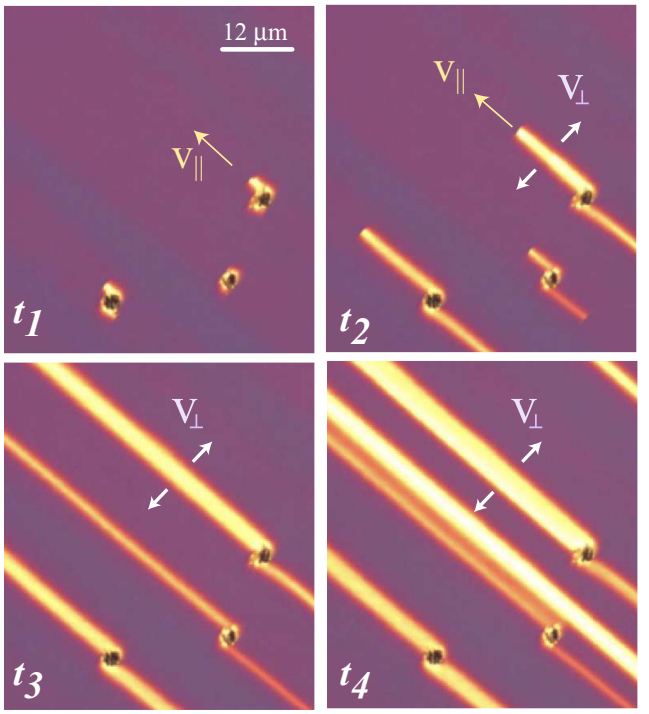

FIG. 4. Finger front propagation. A sequence of snapshots for different instants ($t_1 < t_2 < t_3 < t_4$). Fronts are nucleated from the glass beads, propagating dominantly in the direction orthogonal to the anchoring with a speed $V_\parallel$ and slowly propagating with a speed $V_\perp$ in the direction parallel to the anchoring.

study carried out for a concentration of 16 wt % and a temperature of 32 °C shows the same type of dynamical behaviors.

E. Smectic-*A* phase under the influence of intense voltage

When the sample is on the Sm*A* phase and subjected to an external electrical field no molecular reversal reorientation is observed. As we have mentioned, reorientation fronts are observed near the *N**-Sm*A* transition. When one is far from the transition, inside the Sm*A* phase, fronts and textures can be observed when strong electric fields are applied. Figure 7 illustrates the type of fronts and textures observed. These types of textures are irreversible; when the electric field is turned off, these textures persist. Indeed, the textures and induced dynamics do not correspond to a molecular reorientation. To recover the smectic phase *A*, the sample must be heated to its isotropic phase and slowly cooled to the temperature where smectic phase *A* is observed.

III. THEORETICAL DESCRIPTION

As we mentioned in the previous section near the *N**-smectic-*A* transition, the emergence of intriguing propagative finger fronts is observed. To account for the observed

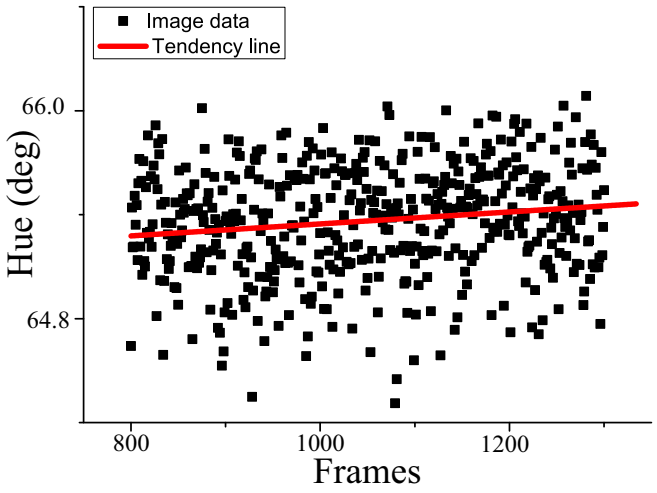

FIG. 5. Hue calibration from a recording video, the analysis area is 12 × 22 pixels. Linear regression fitting of the hue of liquid crystal state for a voltage of 3.9 Vrms. The fitting (red curve) shows a small slope of order $(3.5 \pm 0.9) \times 10^{-4}$. The experimental data dispersion (black square) allows determining the standard deviation associated with the mean value.

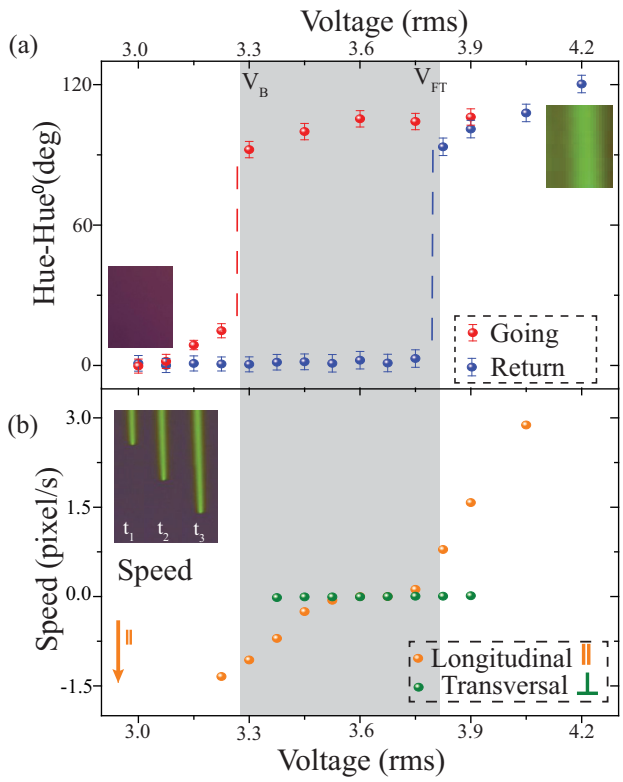

FIG. 6. Experimental bifurcation diagram of reorientational transition of a liquid crystal layer. The painted region stands for the bistable zone. (a) Hue as a function of voltage. The blue and red dots are obtained by increasing and decreasing the voltage applied to the cell. The bars show the standard deviation obtained in the measurements. The insets account for the observed homogenous state, respectively. (b) Front speed as a function of the applied voltage. The orange and green points, respectively, account for the propagation speed orthogonal and parallel to the anchoring of molecules. The inset illustrates a sequence of snapshots that account for the front propagation.

dynamics, we use the strategy based on symmetry arguments and order parameters used by de Gennes to account for the the isotropic-nematic transition [12,13,16]. Note that models similar to the Landau–de Gennes model have been used to describe reorientation transitions induced by electric fields [33,34].

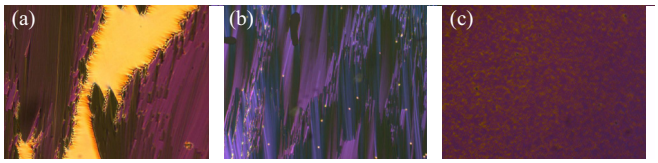

FIG. 7. Irreversible effects on the smectic-*A* phase cell under the influence of intense voltage. Micrographs of a liquid crystal cell obtained by parallel polarized microscopy. (a) Front propagation with a complex boundary of a dark purple texture over a homogeneous phase for a liquid crystal mixture with 16 wt %, at 23 °C and an applied voltage of 25 Vrms. From the above texture and maintaining the applied voltage, the temperature is slowly (b) and abruptly (c) decreased to 20 °C, with a variation rate of 2 °C/min and 20 °C/min, respectively.

Let us introduce the parameter of order $u(x, y, t)$ for the reorientation transition, which, when it is zero, accounts for the planar state of the smectic phase liquid crystal layer, and when it is positive stands for the reoriented state configuration of the smectic phase. The order parameter u satisfies the following equation:

$$\partial_t u = \mu u + \alpha u^2 - u^3 + \delta \partial_{xx} u + \partial_{yy} u, \tag{1}$$

where μ is the bifurcation parameter, which is proportional to the difference between voltage and the Fréederickz voltage, $\mu \propto V - V_{\rm FT}$, in which $V_{\rm FT}$ is the Fréederickz voltage. Besides, this critical parameter depends on the temperature. α accounts for the nonlinear response, which is a function of dielectric permittivity anisotropy, elasticities, conductivities, viscosities, and cell thickness. The last two terms account for elastic coupling, where ∂_{xx} and ∂_{yy} are the Laplacian operators in the respective directions. δ accounts for the elastic anisotropy for the deformations in the different orientations and is a function of the elastic constants, conductivities, viscosities, and cell thickness. The model equation (1) is variational in nature; that is, this equation can be written as

$$\partial_t u = -\frac{\delta \mathcal{F}}{\delta u}, \tag{2}$$

where

$$\mathcal{F} = \int_\Omega \left(-\frac{\mu u^2}{2} - \frac{\alpha u^3}{3} + \frac{u^4}{4} + \frac{\delta (\partial_x u)^2 + (\partial_y u)^2}{2} \right). \tag{3}$$

Hence, the dynamics of the model equation (1) is characterized by the minimization of the functional $\mathcal{F}$.

The model equation (1) has three trivial equilibria:

$$u = u_0 \equiv 0 \tag{4}$$

and

$$u = u_\pm(\alpha, \mu) \equiv \frac{\alpha \pm \sqrt{\alpha^2 + 4\mu}}{2}, \tag{5}$$

where u_0, u_-, and u_+ account for the planar, unstable, and stable reoriented molecular smectic phase configurations [see Fig. 2(b)], respectively. Figure 8 shows the bifurcation diagram of model equation (1). For $\mu < 0$, the planar state is stable, and for $\mu = \mu_T \equiv 0$, the system exhibits a transcritical instability [35], which generates the reoriented phase u_+ as the only stable state (cf. Fig. 8). Therefore, this transition is subcritical in nature. Namely, this transition is discontinuous. The reoriented state u_+ is stable for $\mu \geqslant \mu_{\rm Sn} \equiv -\alpha^2/4$. Then, the system presents coexistence between the planar and the reoriented state, for $-\alpha^2/4 \leqslant \mu \leqslant 0$. Three critical points characterize a subcritical bifurcation: the nascent of bistability $\mu = \mu_{\rm Sn} \equiv -\alpha^2/4$, the transition $\mu = \mu_T = 0$, and the Maxwell point $\mu = \mu_M = -2\alpha^2/9$. This last point is characterized by the fact that the energy of each state is equivalent ($\mathcal{F}[u_0] = \mathcal{F}[u_+]$). Hence, the phase diagram presented by the model equation (1), summarized in Fig. 8, shows a fairly good agreement with the experimental observations (see Fig. 3). Note that model equation (1) qualitatively exhibits the same behavior if the parameters do not change sign. Hence, the

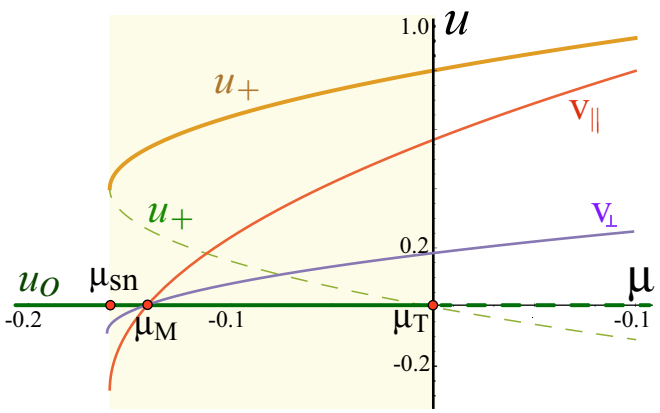

FIG. 8. Bifurcation diagram of model equation (1) by $\alpha = 0.8$ and $\delta = 0.1$. Equilibria u as a function of μ. u_0, u_-, and u_+ account for the planar, unstable, and reoriented molecular smectic phase configuration. Dashed curves account for unstable states. The painted region stands for the bistable zone. $v_\perp$ and $v_\parallel$ are the front speeds in the x and y directions as a function of μ, using formulas (8) and (10), respectively.

particular choice of parameters for the numerical simulations does not change the qualitative dynamics. Then the model equation (1) describes the experimental observations qualitatively well.

Finger propagation

In the bistability region and $\mu > \mu_M$, a localized disturbance of the planar state u_0 generates front propagation [25]. Figure 9 illustrates the typically observed front. The fronts are propagative fingers in the y direction. In this region of parameters, the state u_+ is more stable than the smectic phase u_0; then it invades the system. But as a result of the strong asymmetry in the coupling, this state spreads quicker in one direction than another. Using the notation used in the experiment, the directions y and x correspond to the parallel direction and the perpendicular direction, respectively. The emergence of propagative fingers is observed from the numerical simulations for small δ values where the front propagates faster in the parallel direction than in the perpendicular direction. When considering a random initial condition—where this initial condition is generated by altering the planar state at each point by a Gaussian distribution—the emergence of various propagative fingers is observed. Figure 9(b) depicts a sequence of images of the temporal evolution of model equation (1) with a random initial condition.

To estimate the propagation speed of the fingers, we can consider the following ansatz for a flat front:

$$u(x, y, t) = a\left[1 + \tanh\left(\frac{x - v_\perp t}{2b}\right)\right], \tag{6}$$

where a, b, and $v_\perp$ are parameters that characterize the front. a characterizes the difference between the two equilibria, b is the width of the front, and $v_\perp$ is the front speed.

Replacing this ansatz in Eq. (1) and equating the terms to the different tangent powers, one gets the following relationships:

$$\begin{aligned} \frac{v_\perp a}{2b} + \mu a + \alpha a^2 - a^3 &= 0, \\ -\frac{\delta a}{2b^2} + \mu a + 2\alpha a^2 - 3a^3 &= 0, \\ -\frac{v_\perp a}{2b} + \alpha a^2 - 3a^3 &= 0, \\ \frac{\delta a}{2b^2} - a^3 &= 0. \end{aligned} \tag{7}$$

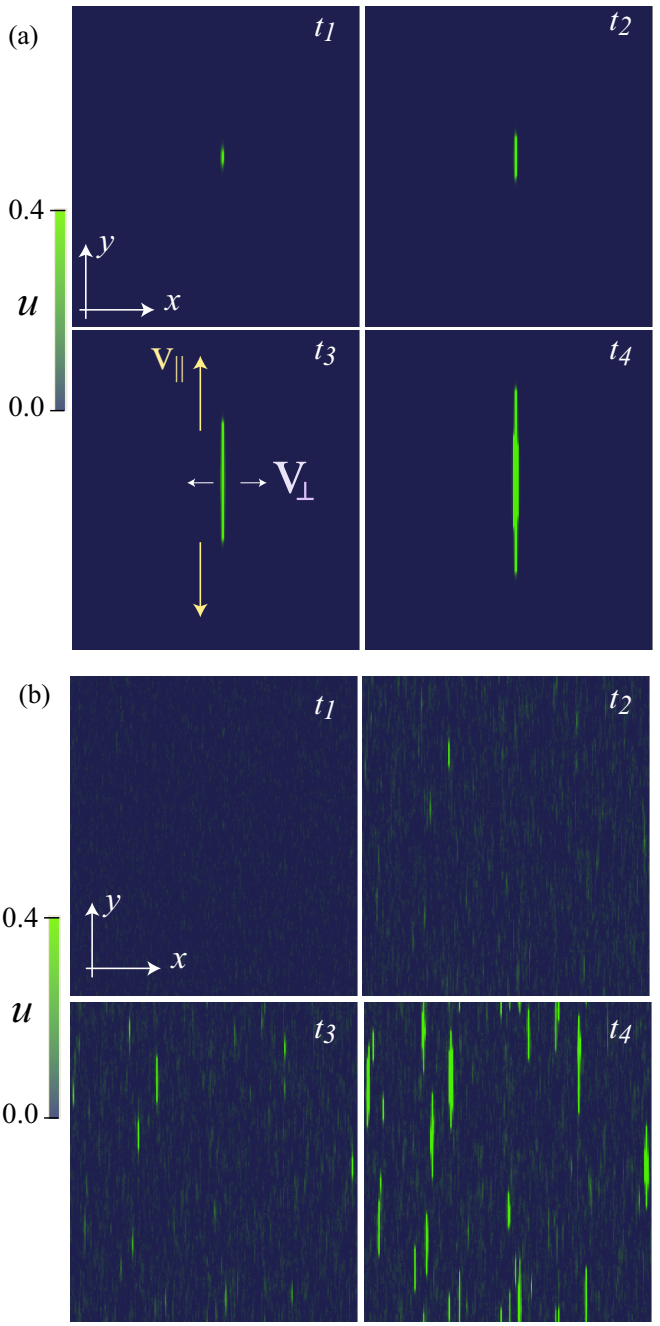

FIG. 9. Front propagation in model equation (1) by $\mu = -0.05$, $\alpha = 0.1$, and $\delta = 0.005$. (a) Temporal sequence from a localized initial condition $t_1 < t_2 < t_3 < t_4$. (b) Temporal sequence from a random initial condition $t_1 < t_2 < t_3 < t_4$.

Using the previous relationships and after straightforward calculations, we get

$$a = \frac{u_+(\alpha,\mu)}{2},$$
$$b = \frac{\sqrt{2\delta}}{2a},$$
$$v_\perp = \alpha\frac{\sqrt{2\delta}}{2} - \frac{3\mu b}{2} = \sqrt{2\delta}\left(\frac{\alpha}{2} - \frac{3\mu}{4a}\right). \tag{8}$$

When one imposes the front speed to be zero, one has that this occurs at the Maxwell point, $\mu = -2\alpha^2/9$. Figure 8 shows the front speed $v_\perp$ as a function of the bifurcation parameter μ. To obtain the front that propagates in the other direction, one can use analogously the same ansatz:

$$u(x,y,t) = a_\parallel\left[1 + \tanh\left(\frac{y - v_\parallel t}{2b_\parallel}\right)\right]. \tag{9}$$

Using the same procedure, one gets

$$a_\parallel = \frac{u_+(\alpha,\mu)}{2},$$
$$b_\parallel = \frac{\sqrt{2}}{2a_\parallel},$$
$$v_\parallel = \alpha\frac{\sqrt{2}}{2} - \frac{3\mu b_\parallel}{2}. \tag{10}$$

Note that the front speed $v_\parallel$ in the direction orthogonal to the molecular anchoring, the y direction, does not depend on the δ parameter. Hence, for a small δ, the front speed in the x direction is δ times smaller than the speed in the y direction. Figure 8 shows the front speed $v_\parallel$ as a function of the bifurcation parameter μ. The curvature of the interface between the two equilibriums can modify the front speed, an effect well known as velocity-curvature or the Gibbs-Thomson effect [3]. This effect can increase the front speed predicted by formula (10).

In brief, model equation (1) gives a fairly good account of the dynamics and the finger propagation observed in the cell of a liquid crystal mixture with planar anchoring near the smectic-*A* to chiral nematic transition [see Fig. 3(b)].

IV. CONCLUSIONS AND REMARKS

We have reported the propagation of finger fronts in anisotropic systems. Based on a cell of a liquid crystal mixture with planar anchoring near the smectic-*A* to chiral nematic transition, when applying a voltage through the cell, we observed the emergence of thin finger fronts that propagate in the direction orthogonal to the anchoring. This front is a manifestation of the molecular reorientation induced by the electric field on the smectic-*A* phase. This phenomenon is known in the literature as the Fréedericksz transition [14]. We use colorimetry characterization to describe the molecular reorientation transition and front dynamics in the liquid crystal cell. This allows us to reveal that the reorientation transition is of the first-order type. The critical points that characterize the transition are established. Then the fronts connect two stable states. Besides, it enables us to characterize the propagation speed as a function of the voltage in different orientations. Theoretically, we have considered a prototype model of transitions in liquid crystals, which qualitatively describes the experimental observations. We have analytically described the bifurcation diagram and the propagation speeds of the finger fronts.

Molecular reorientation transitions induced by electric or magnetic fields are not expected for a smectic-*A* phase since the energetic cost of reorientation destroys the smectic terrace structure. However, close to the *N**-Sm*A* transition, the adjustment of the smectic phase structure allows the observation of reversal reorientation instability driven by an electric field and characterized by finger front propagation.

ACKNOWLEDGMENTS

This work was funded by ANID–Millennium Science Initiative Program–ICN17_012. M.G.C. is thankful for financial support from the Fondecyt 1210353 project. M.J.M. is thankful for financial support from ANID-PAI *Convocatoria Nacional Subvención a Instalación en la Academia Convocatoría 2019*, Folio 77190056. G.G.-C. acknowledges financial support from CONICYT-ANID by Doctorado Nacional No. 2017-21171672.

[1] G. Nicolis and I. Prigogine, *Self-Organization in Non Equilibrium Systems* (Wiley & Sons, New York, 1977).
[2] M. C. Cross and P. C. Hohenberg, Rev. Mod. Phys. **65**, 851 (1993).
[3] L. M. Pismen, *Patterns and Interfaces in Dissipative Dynamics* (Springer, Berlin, 2006).
[4] M. Cross and H. Greenside, *Pattern Formation and Dynamics in Nonequilibrium Systems* (Cambridge University, New York, 2009).
[5] J. Guckenheimer and P. Holmes, *Nonlinear Oscillations, Dynamical Systems, and Bifurcations of Vector Fields* (Springer, New York, 2013).
[6] J. D. Murray, *Mathematical Biology* (Springer-Verlag, Berlin, 1993).
[7] P. Collet and J. P. Eckmann, *Instabilities and Fronts in Extended Systems* (Princeton University, Princeton, NJ, 1990).
[8] Y. Pomeau, Front motion, metastability and subcritical bifurcations in hydrodynamics, Physica D **23**, 3 (1986).
[9] W. van Saarloos and P. C. Hohenberg, Fronts, pulses, sources and sinks in generalized complex Ginzburg-Landau equations, Phys. D (Amsterdam, Neth.) **56**, 303 (1992).
[10] S. Langer, Instabilities and pattern formation in crystal growth, Rev. Mod. Phys. **52**, 1 (1980).
[11] P. G. Saffman, Viscous fingering in Hele-Shaw cells, J. Fluid Mech. **173**, 73 (1986).

[12] S. Chandrasekhar, *Liquid Crystals* (Cambridge University, New York, 1992).
[13] P. G. de Gennes and J. Prost, *The Physics of Liquid Crystals*, 2nd ed. (Clarendon, Oxford, 1993).
[14] V. Fréedericksz and V. Zolina, Forces causing the orientation of an anisotropic liquid, Trans. Faraday Soc. **29**, 919 (1933).
[15] A. Rapini, Instabilités magnétiques d'un smectique C, J. Phys. Fr. **33**, 237 (1972).
[16] I. M. Blinov and V. Chigrinov, *Electroptic Effects in Liquid Crystal Materials* (Springer-Verlag, Berlin, 1994).
[17] S. J. Elston, Smectic-*A* Fréedericksz transition, Phys. Rev. E **58**, R1215(R) (1998).
[18] M. J. Morel, U. Bortolozzo, M. G. Clerc, A. Jullien, and S. Residori, Colorimetry characterization of molecular reorientation transition in thin nematic cells, Chaos **30**, 073102 (2020).
[19] D.-K. Yang and S.-T. Wu, *Fundamentals of Liquid Crystal Devices* (Wiley & Sons, Hoboken, NJ, 2006).
[20] M. L. Parra, P. I. Hidalgo, and E. Y. Elgueta, Synthesis and mesomorphic properties of oxadiazole esters derived from (*R*)-2-octanol, (*S*)-2-*n*-octyloxypropanol and (2*S*, 3*S*)-2-chloro-3-methylpentanol, Liq. Cryst. **35**, 823 (2008).
[21] N. H. Hartshorne and A. Stuart, *Crystals and the Polarising Microscope* (Arnold, London, 1970).
[22] S. Echeverría-Alar and M. G. Clerc, Labyrinthine patterns transitions, Phys. Rev. Research **2**, 042036(R) (2020).
[23] I. Dierking, *Textures of Liquid Crystals* (Wiley & Sons, Hoboken, NJ, 2003).
[24] M. Ismaïli, A. Anakkar, G. Joly, N. Isaert, and H. T. Nguyen, Multicritical behaviors and an induced twist grain boundary phase in a binary liquid crystalline mixture, Phys. Rev. E **61**, 519 (2000).
[25] M. G. Clerc, S. Residori, and C. Riera, First-order Fréedericksz transition in the presence of a light driven feedback, Phys. Rev. E **63**, 060701(R) (2001).
[26] B. J. Frisken and P. Palffy-Muhoray, Electric-field-induced twist and bend Fréedericksz transitions in nematic liquid crystals, Phys. Rev. A **39**, 1513 (1989).
[27] B. J. Frisken and P. Palffy-Muhoray, Freedericksz transitions in nematic liquid crystals: The effects of an in-plane electric field, Phys. Rev. A **40**, 6099 (1989).
[28] S. Garg, S. Saeed, and U. D. Kini, Effect of a stabilizing magnetic field on the electric-field-induced Fréedericksz transition in 4-*n*-pentyl-4-cyanobiphenyl Phys. Rev. E **51**, 5846 (1995).
[29] S. D. Durbin, S. M. Arakelian, and Y. R. Shen, Optical-Field-Induced Birefringence and Freedericksz Transition in a Nematic Liquid Crystal, Phys. Rev. Lett. **47**, 1411 (1981).
[30] A. J. Karn, S. M. Arakelian, Y. R. Shen, and H. L. Ong, Observation of Magnetic-Field—Induced First-Order Optical Fréedericksz Transition in a Nematic Film, Phys. Rev. Lett. **57**, 448 (1986).
[31] B. Wen and C. Rosenblatt, First-Order Fréedericksz Transition Above the Nematic–Smectic-*A* Phase Transition, Phys. Rev. Lett. **89**, 195505 (2002).
[32] J. B. Poursamad and T. Hallaji, Freedericksz transition in smectic-A liquid crystals doped by ferroelectric nanoparticles, Phys. B: Condens. Matter **504**, 112 (2017).
[33] M. G. Clerc, A. Petrossian, and S. Residori, Bouncing localized structures in a liquid-crystal light-valve experiment, Phys. Rev. E **71**, 015205(R) (2005).
[34] K. Alfaro-Bittner, C. Castillo-Pinto, M. G. Clerc, G. González-Cortés, R. G. Rojas, and M. Wilson, Front propagation into an unstable state in a forced medium: Experiments and theory, Phys. Rev. E **98**, 050201(R) (2018).
[35] S. H. Strogatz, *Nonlinear Dynamics and Chaos with Student Solutions Manual: With Applications to Physics, Biology, Chemistry, and Engineering* (Westview, Boulder, CO, 2015).